Liquid Crystals
Publication details, including instructions for authors and subscription information:
http://www.informaworld.com/smpp/title~content=t713926090

Optical pattern simulations for closed cylinders of liquid crystals

B. -J. Liang[a]; J. -G. Wei[a]; Shu-Hsia Chen[a]
[a] Institute of Electro-Optical Engineering, National Chiao Tung University, Taiwan, Republic of China

To cite this Article Liang, B. -J. , Wei, J. -G. and Chen, Shu-Hsia(1993) 'Optical pattern simulations for closed cylinders of liquid crystals', Liquid Crystals, 14: 5, 1553 — 1560
To link to this Article: DOI: 10.1080/02678299308026467
URL: http://dx.doi.org/10.1080/02678299308026467

LIQUID CRYSTALS, 1993, VOL. 14, NO. 5, 1553–1560

Optical pattern simulations for closed cylinders of liquid crystals

by B.-J. LIANG, J.-G. WEI and SHU-HSIA CHEN*
Institute of Electro-Optical Engineering, National Chiao Tung University, Hsinchu, Taiwan 300, Republic of China

Optical patterns for the polarizing microscope textures of closed cylinders of liquid crystals (CCLCs) are studied by the Jones vector formulation. The simulated director configuration diagram of a CCLC with normal orientation at the walls contains four kinds of stable director configurations. The resulting texture under some approximations depends only on phase shifts. The patterns are characterized by dark brushes that coincide with the directions of the crossed polarizers. Additionally, there are concentric circle fringes. For the ring defect structure, the centre region of the cylinder exhibits a black extinction. However, this is not distinguishable as between the hyperbolic and radial structures for both the point and the ring defect patterns. Comparing the observed patterns with the simulated ones, we find that the dark cross brushes and the centre black extinction of simulated patterns are similar to those that are observed. However, the concentric circle fringes of the observed pattern are not in accordance with the simulated pattern.

1. Introduction

Optical microscopy is a popular tool for investigating anisotropic structures [1–2]. From the optical patterns observed using crossed polarizers, we have reported the first study of the stability of a closed cylinder of liquid crystal (CCLC) [3]. Homeotropic cylindrical cavities for the CCLCs are formed by coating DMOAP (*N*,*N*-dimethyl-*N*-octadecyl-3-aminopropyltrimethoxysilyl chloride) on two flat substrates, one having cylindrical cavities in it. The 5CB (4′-*n*-pentyl-4-cyanobiphenyl) is then filled between the two flat substrate plates. The cell textures are examined from the top view of the cylinder using crossed polarizing microscopy. The behaviour of the texture is not changed on rotating the sample between crossed polarizers. Due to the different radii of the cylinders, the observed patterns can be separated into two kinds. For a smaller radius cylinder, the optical patterns are shown in figure 1; figures 1 (*a*) and (*b*) refer to cells with height, $2D = 4{\cdot}1\,\mu$m and radii, $R = 2{\cdot}65$ and $6{\cdot}5\,\mu$m, respectively. The characteristic extinction cross coincides with the directions of the polarizers. Both cells exhibit the same behaviour. For the larger radius, the optical patterns are shown in figure 1 (*c*) in which R is $29\,\mu$m and $2D$ is about $5{\cdot}1\,\mu$m. It is found that each cylinder presents four extinction branches originating from the centre of the optical pattern and oriented along the directions of the plarizers. The centre region of the cylinder exhibits a black extinction. This demonstrates the physical meaning that the field of the director **n** is normal to both bases of the cylindrical cavity [4]. The observations also demonstrate that the three cells have normal molecular configurations with the directors lying on the diametrical section.

A nematic liquid crystal (NLC) confined to a small cavity exhibits a specific director configuration, depending on the defined cavity shape, the elastic constants and the surface boundary conditions [5–7]. In this paper, we consider that the NLC in CCLCs

* Author for correspondence.

0267–8292/93 $10·00

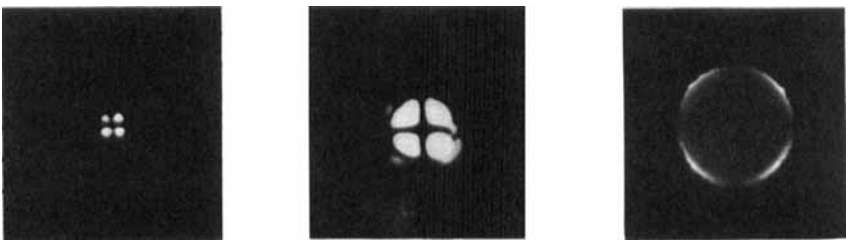

(*a*) (*b*) (*c*)

Figure 1. Three CCLCs with NLC, 5CB, viewed between crossed polarizers, where (*a*) $D = 2{\cdot}05\,\mu m$ and $R = 2{\cdot}65\,\mu m$, (*b*) $D = 2{\cdot}05\,\mu m$ and $R = 6{\cdot}5\,\mu m$, and (*c*) $D = 2{\cdot}55\,\mu m$ and $R = 2{\cdot}9\,\mu m$.

is rigidly and perpendicularly anchored to the boundaries. It will be emphasized that the geometrical boundaries of a CCLC consist of three parts: the upper and lower bases, and the lateral surface of the cylinder. We have reported the first study of a single volume singular point existing alone in a CCLC cell [3]. There are two types of possible molecular configuration, namely, the hyperbolic and radial structures. Typically, the calculated configurations of these two types are shown in figure 2. On increasing the aspect ratio of the cavity, an annular phenomenon is observed. An annular structure was noted by Erdmann [8] and Kralj [9] in droplets and by Vilfan [10] in a capillary in which the only boundary treated was the lateral surface of the cylinder. However, we are the first to explore the annulus structure for CCLC. This annular phenomenon is due to the formation of a disclination ring structure [4]. Comparing the total free energy of various probably molecular configuration, we can obtain the stability of the director in a CCLC, depending not only on the aspect ratio, Γ (Γ defined as R/D) of the cylinder but also on K_{33}/K_{11} (bend to splay Frank elastic constants ratio) for the NLC. A director configuration diagram [11] of the CCLC is then calculated; it contains four kinds of possible director configurations which are called the hyperbolic point, the radial point, the hyperbolic ring and the radial ring configurations.

In this paper, a general description of the propagation of light through the CCLC will be discussed. The optical response characteristics of a CCLC are shown to depend strongly upon the NLC director configuration. It is necessary to calculate microscope textures for a variety of different suspected director configuations in order to provide for better CCLC characterization. If the molecular director is related to the optical axis, a predicted micrograph can be generated from the theoretical structures of the director configuration [12].

To find the exact optical patterns that would be produced by these molecular configurations requires the assumption that the geometry of a CCLC is close to locally translational invariance [7–9], that is, that the rate of change of the molecular configuration with distance is small. The NLC is considered to have principal refractive indices n_e (extraordinary) and n_o (ordinary) and the optical axis parallel to the local nematic director **n**. Because $n_e - n_o \ll n_e, n_o$, reflections and deviations of the light rays caused by refraction in any internal NLC structure are neglected. Besides, we ignore reflections on the CCLC surface and diffraction effects. In this paper, we only simulate the textures of normal molecular configurations with the directors lying on the diametrical section. The resulting texture under these approximations will therefore depend only on phase shifts.

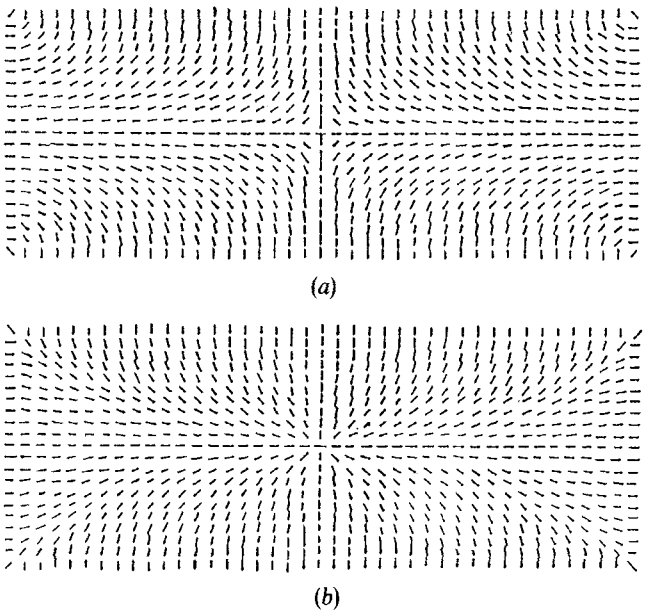

Figure 2. When $D = 2{\cdot}5\ \mu m$, $R = 6{\cdot}5\ \mu m$, and (*a*) $K_{13} = 0{\cdot}74$, the hyperbolic hedgehog is stable on the diametrical section. (*b*) with $K_{13} = 0{\cdot}5$, the radial configuration is stable.

2. General formulations

The optical behaviour of a CCLC sample in the diametrical section is modelled by dividing the material into an array of elements, $(m+1)$ by $(n+1)$, which are shown in figure 3. Each element is assumed to be uniaxially birefringent, with a uniform optic axial direction. This optic axial direction can vary from element to element [12].

When an optical system consists of many elements, each oriented at a different angle, the calculation of the overall transmission becomes simplified by Jones calculus. The Jones calculus is a powerful 2×2 matrix method in which the state of polarization is represented by a two component vector and each optical element is represented by a 2×2 matrix. The overall matrix for the whole system is obtained by multiplying all matrices, and the polarization state of the transmitted light is computed by multiplying the vector representing the input beam by the overall matrix [13].

The sample is placed between a pair of crossed polarizers. If the angle between the polarizer and the observed diametrical direction is represented by φ, the transmittance T of the ith element will be given by

$$T_i = \sin^2 2\varphi \sin^2 (\gamma_i/2), \tag{1}$$

where γ_i is the total phase shift at the ith element. For various φ and with i from 0 to n substituted into equation (1), then the complete texture will be determined.

3. Pattern generations

The calculated optical pattern of a CCLC placed between crossed polarizers is generated by the optical formulation for the director configuration of the structure [6]. In this section, textures simulated by both monochromatic light and white light will be created. In all of our calculations we use typical values for $n_0 = 1{\cdot}54$, $n_e = 1{\cdot}7$, and $K_{33}/K_{11} = 1{\cdot}35$ of NLC 5CB.

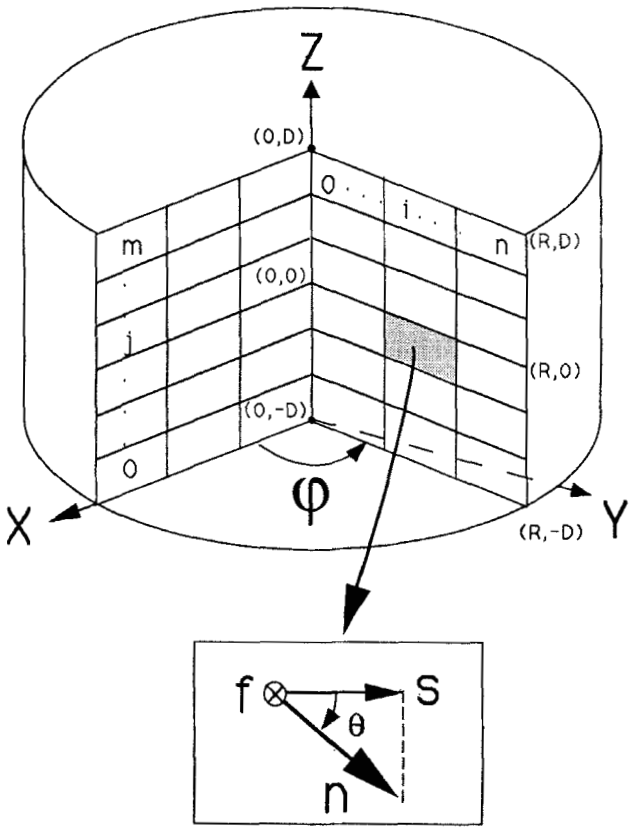

Figure 3. The coordinate system and schematic diagram of an array of cells.

3.1. *Monochromatic light simulated textures*

In previous optical formulations, monochromatic light is assumed and we put $\lambda = 0{\cdot}509\ \mu m$.

For a small aspect ratio of the CCLC, the point defect is stable. The simulated optical patterns of the hyperbolic point and radial point structure are shown in figure 4. The half height of the cylinder is $2{\cdot}1\ \mu m$. Figures 4 (*a*) and (*b*) refer to the hyperbolic and the radial point structures both with $R = 2{\cdot}65\ \mu m$. For $R = 6{\cdot}5\ \mu m$, figures 4 (*c*) and (*d*) refer to the hyperbolic and the radial point structures, respectively. The patterns are characterized by dark brushes that lie parallel to the directions of the crossed polarizers. In addition to the dark brushes, there also exist concentric circle fringes. These result from the optical path difference between extraordinary (e) and ordinary (o) rays. In these simulated optical patterns, the hyperbolic and radial point structures are indistinguishable. It is also found that the grey level for $R = 6{\cdot}5\ \mu m$ is more gradual than for $R = 2{\cdot}65\ \mu m$.

For a larger aspect ratio, the disclination ring structures are stable. Figures 4 (*e*) and (*f*) refer to the hyperbolic and the radial ring structures both with $R = 25 \mu m$ and $D = 2{\cdot}5\ \mu m$. The patterns are also characterized by cross dark brushes and concentric circle fringes. In addition to these characteristics, the centre region of the cylinder exhibits a black extinction. In these simulated optical patterns of ring structures, the hyperbolic and radial structures are also indistinguishable.

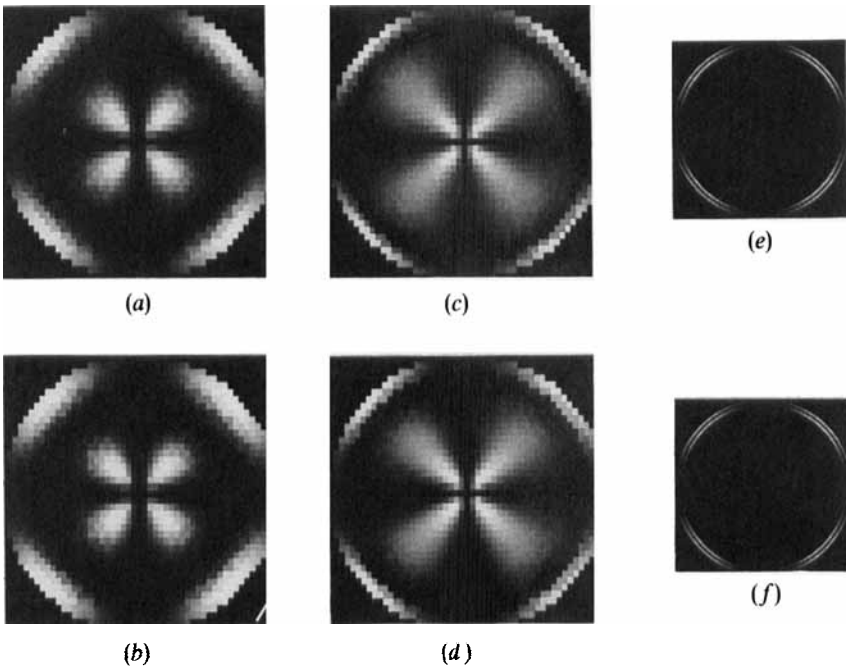

Figure 4. Monochromatic simulation of polarizing microscope textures with $D = 2{\cdot}1\ \mu m$ and $R = 2{\cdot}65\ \mu m$ for, (*a*) hyperbolic and (*b*) radial, point structures; $D = 2{\cdot}1\ \mu m$ and $R = 6{\cdot}5\ \mu m$ for (*c*) hyperbolic and (*d*) radial, point structures; $D = 2{\cdot}55\ \mu m$ and $R = 25\ \mu m$ for (*e*) hyperbolic and (*f*) radial, ring structures.

3.2. *Optical patterns under different aspect ratios*

It is well known that the concentric circle fringes result from the difference of optical path between the e-ray and o-ray [14]. The optical path difference is a function of the thickness and birefringence of the CCLC. In this section, we also use 5CB but now it is confined in a cylinder with a different aspect ratio. According to the director configuration diagram calculated in [6], one can directly know, for certain circumstances, what the most probable stable configuration is. We chose the stable hyperbolic point structures, $D = 1$ and $D = 4\ \mu m$, both with $R = 3\ \mu m$ which refer to figures 5 (*a*) and (*b*), respectively. The conditions of the stable radial ring configuration are $D = 1$ and $D = 4\ \mu m$ both with $R = 25\ \mu m$ referring to figures 5 (*c*) and (*d*). For $D = 1\ \mu m$, there is no dark concentric circle for both point (see figure 5 (*a*)) and ring (see figure 5 (*c*)) defect structures. For $D = 2{\cdot}5\ \mu m$, there is one dark concentric circle for point (see figures 4 (*a*) and (*c*)) and ring (see figure 4 (*f*)) defect structures. For $D = 4\ \mu m$, there are two dark concentric circles for both point (see figure 5 (*b*)) and ring (see figure 5 (*d*)) defect structures. The reason is that light with an optical path difference of $p\lambda$, where p is an integral number, results in a circle of darkness (zero illumination) for all azimuths. It is then obvious that the greater the thickness is, the larger the number will be of concentric rings found.

3.3. *White light simulated textures*

The light used in our observations was provided by a tungsten halogen lamp which is a white light source. Therefore, we are able to simulate white light. Instead of simulating a full colour texture obtained with white light using laws of colour mixing,

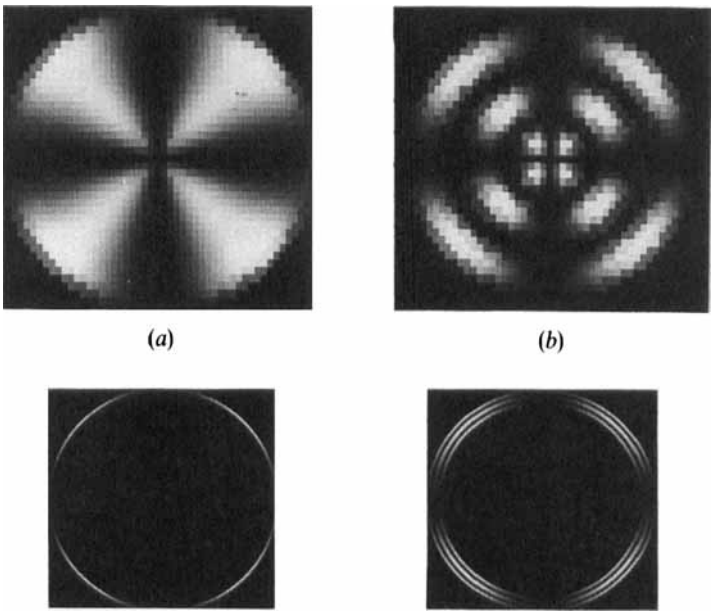

Figure 5. Monochromatic simulation of polarizing microscope textures for stable configurations at different aspect ratios of the cylinder. $R = 3\ \mu m$ and (*a*) $D = 1\ \mu m$ and (*b*) $D = 4\ \mu m$ for hyperbolic point structures. $R = 25\ \mu m$ and (*c*) $D = 1\ \mu m$ and (*d*) $D = 4\ \mu m$ for radial ring structures.

we simulate a black and white (BW) photograph by combining the textures at different wavelengths [1]. A wavelength of 0·535 μm approximately receives a 60 per cent weighting. A weighting of 20 per cent as assigned to both 0·47 and 0·6 μm wavelength light. In the following simulated optical patterns of both point and ring structures, the hyperbolic and radial structures are also indistinguishable. Therefore, we only show the stable textures for different aspect ratios.

The simulated optical patterns of the point and ring defect structures are shown in figure 6. Figures 6 (*a*) and (*b*) with 2·1 μm as the half height of the cylinder refer to the hyperbolic structures with $R = 2{\cdot}65$ and $R = 6{\cdot}5\ \mu m$, respectively. Figure 6 (*c*) is the radial disclination ring structure. The patterns are also characterized by cross dark brushes and concentric circle fringes. For the ring defect structure, the centre region of the cylinder also exhibits a black extinction. It is found that the contrast of the light simulated by white light is more gradual than that given by monochromatic light.

4. Comparing generated patterns with observed ones

We can compare the observed point structure patterns in figures 1 (*a*) and (*b*) with the simulated optical patterns in figures 6 (*a*) and (*b*) with the same aspect ratios. It is obvious that these patterns are similarly characterized by dark brushes that lie parallel to the directions of the crossed polarizers. For the defect structure, the observed pattern in figure 1 (*c*) is compared with the optical simulated pattern in figure 6 (*c*). Both patterns are also characterized by dark brushes that lie parallel to the directions of the crossed polarizers and the centre regions of the cylinders also exhibit a black extinction.

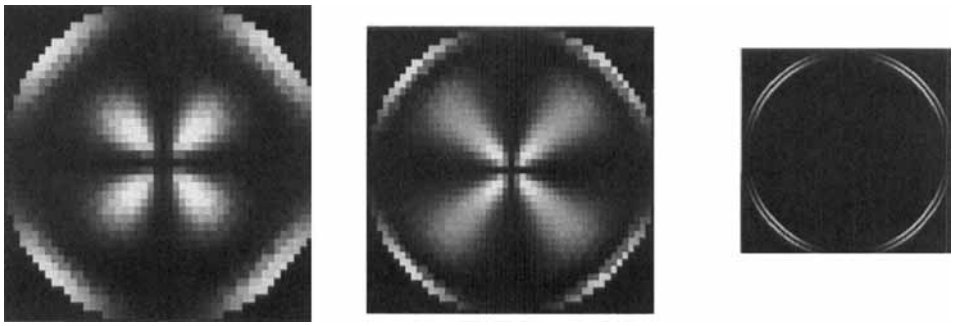

(*a*) (*b*) (*c*)

Figure 6. White light simulation of polarizing microscope textures for stable structures for which (*a*) $D = 2{\cdot}1\ \mu m$ and $R = 2{\cdot}65\ \mu m$ for the hyperbolic point structure, (*b*) $D = 2{\cdot}1\ \mu m$ and $R = 6{\cdot}5\ \mu m$ for the hyperbolic point structure, and (*c*) $D = 2{\cdot}55\ \mu m$ and $R = 25\ \mu m$ for the radial ring structures.

In the above comparison, the cross dark brushes and the centre black extinction are similar, but this concentric circle fringes of the observed pattern for both the point and ring defect structures are not in accordance with the simulated patterns. This is caused by two reasons: (i) there is no strong molecular anchoring on the surface [9]; (ii) the variation of the optical path difference. The optical path difference between the e-ray and the o-ray results from the height of the cylinder and the total birefringence of the CCLC. The height of the experimental CCLCs is measured by a surface profile measuring system for the cavities of the CCLCs. After assembling the sample, the height of the CCLC will be larger than the measured height. The variation of the height will result in the optical path difference in the observation being larger than that found in the calculation. The number of concentric circle fringes of the observed pattern will be greater than that of the simulated patterns. In fact, the results are the reverse. Thus, the influence on the variation of the optical path difference is due to the total birefringence of the CCLC. Considering our processes of sample preparation, we utilize wet etching to etch cavities. The etched surfaces on the lateral sides of the cavities will not be perpendicular to the bases of the cavities. Therefore, the model describing the experimental sample will be modified.

5. Conclusion

The use of microscopy to study director configuration is clearly limited to the diameter of the CCLCs, which need to be sufficiently larger than the wavelength of the light used in order to see textural detail. We utilize the Jones vector formulation for simulating the polarization microscope textures of CCLCs. In the simulations, we predicted optical patterns resulting from these calculated configurations. Hyperbolic point, hyperbolic ring, radial point, and radial ring patterns were studied. The patterns are characterized by dark brushes that lie parallel to the directions of the crossed polarizers and concentric circle fringes. The number of the concentric fringes is determined by the optical path difference between the e-ray and the o-ray. For the ring defect structure, the centre region of the cylinder exhibits a black extinction. However, it is indistinguishable as between the hyperbolic and radial structure in both the observed and the simulated patterns. The concentric circle fringes of the observed patterns, for both the point and ring defect structures, are not in accordance with the

simulated patterns. The most likely reason is that the lateral surfaces of the cavities are not perpendicular to the bases of the cavities.

This research was supported in part by the Chinese National Science Council under Contract No. NSC-81-0208-M-009-516.

References

[1] ONDRIS-CRAWFORD, R., BOYKO, E. P., WAGNER, B. G., ERDMANN, J. H., ZUMER, S., and DOANE, J. W., 1991, *J. appl. Phys.*, **69**, 6380.
[2] CRAWFORD, G. P., MITCHELTREE, J. A., BOYKO, E. P., FRITZ, W., ZUMER, S., and DOANE, J. W., 1992, *Appl. Phys. Lett.*, **60**, 3226.
[3] CHEN, S.-H., and LIANG, B.-J., 1991, *Appl. Phys. Lett.*, **59**, 1173.
[4] LIANG, B.-J., and CHEN, S.-H., 1991, *Jpn. J. appl. Phys. part 2*, **30**, L1955.
[5] DUBOIS-VIOLETTE, E., and PARODI, O., 1969, *J. Phys., Paris*, **C4**, 57.
[6] VOLOVIK, G. E., 1983, *Sov. Phys. JETP*, **58**, 1159.
[7] WILLIAMS, R. D., 1986, *J. Phys.* A, **19**, 3211.
[8] ERDMANN, J. H., ZUMER, S., and DOANE, J. W., 1990, *Phys. Rev. Lett.*, **64**, 1907.
[9] KRALJ, S., and ZUMER, S., 1992, *Phys. Rev.* A, **45**, 2461.
[10] VILFAN, I., VILFAN, M., and ZUMER, S., 1991, *Phys. Rev.* A, **43**, 6875.
[11] LIANG, B.-J., and CHHN, S.-H., 1992, *J. appl. Phys.*, **71**, 2189.
[12] NICHOLSON, T.M., 1989, *Molec. Crystals liq. Crystals*, **177**, 163.
[13] YARIV, A., and YEH, P., 1984, *Optical Waves in Crystals* (John Wiley & Sons), Chap. 5.
[14] WAHLSTROM, E. E., 1969, *Optical Crystallography* (John Wiley & Sons), Chap. 10.